Studying the Smelting Behavior of Bauxite Residue Pellets Reduced by Hydrogen using High Temperature Thermal Analysis

D, Hariswijaya[1] and J. Safarian[2]

1.PhD candidate, Norwegian University of Science and Technology, Trondheim Norway 7034. Email: dali.hariswijaya@ntnu.no
2. Professor, Norwegian University of Science and Technology, Trondheim Norway 7034. Email: jafar.safarian@ntnu.no

Keywords: Bauxite residue, Circular economy, Hydrogen reduction, Thermal analysis

ABSTRACT

Treating bauxite residue as an alternative source of metals for iron and aluminium industry is an approach to promote circular economy in metal industries. Reduction of metal oxides with H_2-based process is an important step on decarbonization of metal industry. In this study bauxite residue pellets were prepared and were reduced with different H_2-H_2O gas compositions at different temperatures which yielded with various degrees of reduction. The bauxite residue pellets were made from a mixture of bauxite residue and $Ca(OH)_2$ powders and sintered at 1150°C. Hydrogen reduction was carried out on the oxide pellets using a resistance furnace at elevated temperatures in controlled reduction atmosphere of H_2-H_2O gas mixtures which resulted in reduction of iron oxides in the pellets. Unreduced and reduced pellets were subsequently heated to 1400°C to study their smelting behaviour using Differential Thermal Analysis (DTA) and Thermogravimetric Analysis (TGA) technique to investigate the evolution of phases related to slag formation via smelting. Equilibrium module of Factsage™ was utilized to analyse results of thermal analysis. It was observed that Tricalcium phosphate-β (CaP_2O_8), Bredigite ($Ca_7Si_4MgO_{16}$), Rankinite ($Ca_3Si_2O_7$), and calcium alumino ferrite ($Ca[Al,Fe]_6O_{10}$) were formed during thermal analysis as intermediate phases. The initial slag formation for sintered and reduced pellets occurred at 900 °C which mainly contains calcium and small amount of strontium component. The slag formation rate increases significantly starting from 1100 °C when iron oxides started to form initial molten slag phase which then followed by other oxides dissolution in the system. Gas formation was observed at 1180 °C, and it was found that the gas to be released from unreduced pellets is O_2 meanwhile the l gas to be released from reduced pellets is SO_2 gas. Gas formation rate for both pellets start to increase at 1280 °C when the remaining chemically bonded gas start to be released from the system.

INTRODUCTION

Bayer Process and Bauxite Residue

The Bayer process was invented and patented by Carl Josef Bayer in 1888 and has since then been the leading process for alumina (Al_2O_3) production in the world. The process consists of eight main stages: Milling, desilication, digestion, clarification, precipitation, evaporation, classification, and calcination. In the milling step, the bauxite ore is crushed down into finer particles. Additionally, limestone is added to create a pumpable slurry. After the milling step, the slurry moves through a process called desilication, which involves removing silica (SiO_2). The slurry is then digested using a NaOH solution, which dissolves the aluminium bearing minerals in the bauxite. These minerals include gibbsite ($Al(OH)_3$, boehmite (γ-AlO(OH)) and diaspore (α-AlO(OH)). When the solution is added, the following reactions take place with gibbsite and boehmite/diaspore, given by equation (1) and equation (2) respectively (Smallman and Bishop, 1999).

$$Al(OH)_{3(s)} + NaOH_{(aq)} \rightarrow Al(OH)^-_{4(aq)} + Na^+_{(aq)} \quad (1)$$

$$AlO(OH)_{(s)} + NaOH_{(aq)} + H_2O_{(l)} \rightarrow Al(OH)^-_{4(aq)} + Na^+_{(aq)} \quad (2)$$

After the processing step, the slurry is cooled down using a series of flash tanks at 1 atm. The slurry is then prepared for clarification where the bauxite residue (BR) is separated away through

sedimentation, where chemical additives assist in driving the BR to the bottom of the settling tanks. BR is transferred to washing tanks, where the goal is to recover the caustic soda used in the digestion step. The saturated liquid undergoes a series of filtration steps and BR is left in disposal areas. After clarification, alumina is recovered through crystallization during precipitation step. The precipitation reaction is shown in equation (3) (Smallman and Bishop,1999).

$$Al(OH)^{-}_{4(aq)} + Na^{+}_{(aq)} \rightarrow Al(OH)_{3(s)} + NaOH_{(aq)} \quad (3)$$

Evaporation of the liquid used during crystallization takes place in heat exchangers, where it is subsequently cooled down afterwards in flash tanks. The condensate that is created through this process is re-used for BR washing or as feed water. Recovered caustic soda is then re-added to the digestion step. The crystals are classified into size ranges, using cyclones and gravity classification tanks. For the coarse crystals, separation from liquid and calcination is performed. For the finer crystals, washing to remove organic impurities and re-addition to the precipitation step is performed. Calcination of the coarse crystals is done by roasting in calciners. The roasting process takes place at temperatures up to 1100 °C. This drives off moisture and water, which eventually creates alumina solids. The calcination reaction is shown in equation (4) (Smallman and Bishop,1999).

$$2Al(OH)_{3(s)} \rightarrow Al_2O_{3(s)} + 3H_2O_{(g)} \quad (4)$$

Smelting Reduction of Bauxite Residue

Red mud, also known as bauxite residue (BR) in dewatered form, is the main by-product generated in the Bayer process. Typically, for each tonne of produced alumina from bauxite ore, about 1.5 tonnes of BR is produced (Pandey and Prakash, 2020). The generated BR from the Bayer process is stored in large holding ponds, where only 1% to 2% is being recycled (Brunori et al., 2005). Dried BR typically contains up to 50% of iron oxides. Other compounds found in BR includes silica oxides, titanium oxides, aluminium oxides, and other oxides. It is also highly alkaline, with a pH level ranging from 12-13. Due to its high alkalinity, red mud that is stored away in holding ponds poses a great environmental threat to its surroundings. The main way of treating the alkaline BR, is to attempt neutralizing by adding acidic substances, such as HCl (Brunori et al., 2005).

Smelting reduction of BR opens opportunities for recovery of its metal content, especially iron (Liu et al., 2021), aluminium (Lazou et al., 2021) and rare-earth elements (REEs) (Borra et al., 2016). It is to be understood from previous research that removal of iron content is a necessary preliminary step for effective recovery of alumina and REEs in BR (Lazou et al., 2021; Borra et al., 2016) and smelting reduction is believed to be the most efficient method for removal of iron in BR. Several studies on smelting reduction of BR have been conducted within the past decade which mainly tries to recover iron content in BR either in the form of magnetite (Lazou et al., 2017) or metallic iron (Kar, van der Eijk and Safarian, 2022; Skibelid et al., 2022; Lazou et al., 2021; Ekstroem et al., 2021; Borra et al., 2016).

Smelting reduction of BR with H_2 at low temperature (480 °C) was able to produce magnetite with 87% conversion degree with insignificant metallic iron production (Samouhos et al., 2017). Meanwhile smelting reduction with H_2 at high temperature (1000 °C) was able to completely reduce Fe content in BR to metallic Fe (Kar, van der Eijk and Safarian, 2022; Skibelid et al., 2022). However, the recovery of Fe-containing phases from solid-state reduced BR remains an issue due to its physical nature which exists in miniscule spots with less than 20 µm in particle diameter (Kar, van der Eijk and Safarian, 2022; Skibelid et al., 2022). Carbothermic reduction of BR beyond Fe melting point (>1538 °C) was able to reliably produce pig iron in its own separated phase (Lazou et al., 2021; Ekstroem et al., 2021). The remaining issue was recovery of Al content from its slag where almost half of it was trapped in Gehlenite ($Al_2Ca_2O_7Si$) phase which is difficult to recover via hydrometallurgical means (Lazou et al., 2021).

Previous studies showed that temperature of smelting reduction plays a key role in determining final phase composition and state of reduced BR. Smelting reduction beyond Fe melting point can reliably produce pig iron in separated phase, but it will also produce unleachable slag which significantly lowers its valorisation potential. Meanwhile heat treating in solid state has its own challenges which mainly revolves around separation process of metallic iron which distributed throughout BR in miniscule spots (Kar, van der Eijk and Safarian, 2022; Skibelid et al., 2022). Thus, the aim of present

study is to assess change in phase compositions of BR and smelted BR with increasing temperature through comparison of experimental data and thermochemistry simulation.

MATERIALS AND METHODS

An experimental procedure was designed to study smelting behaviour of BR pellets which has been reduced by hydrogen. A mix of BR and $Ca(OH)_2$ was made and pelletized, then they were sintered. The sintered pellets were reduced under different H_2-H_2O gas mixtures. X-ray Diffraction (XRD) and X-ray Fluorescence (XRF) were employed to analyse phase composition of sintered pellets, meanwhile only XRD was employed to analyse phase composition of reduced pellets. A single pellet from the sintered pellets and reduced pellets was then crushed and sieved under 1 mm for Differential Thermal Analysis (DTA) and Thermogravimetric analysis (TGA) to analyse smelting behaviour of sintered and reduced pellets with increasing temperature up to 1400 °C.

Pelletizing and Sintering

BR fines were deagglomerated and screened (< 250 μm) to obtain uniform sizing on the mixing process. Raw $CaCO_3$ powder was calcined to make CaO powder. Resulting CaO powder was grinded and screened (< 250 μm) before it was hydrated to make $Ca(OH)_2$ powder. BR fines were mixed with $Ca(OH)_2$ powder with a mass ratio of 1:0.38 respectively. The ratio was decided based on the stoichiometric ratio of CaO needed to effectively produce calcium aluminate phase in the reduced pellets to allow effective recovery of alumina through leaching. The green pellets were made using a disc pelletizer and screened to obtain pellets with diameter of 4-10 mm which then air-dried for 1 day and subsequently sintered at 1150 °C for 2 hours in a muffle furnace. The sintered pellets were cooled down naturally inside the furnace for 8 hours before taken out. Flowsheet of the pelletizing and sintering process is shown in FIG 1, meanwhile XRF analysis of raw BR, $CaCO_3$ powder and sintered pellet are shown in Table 1, Table 2, and Table 3, respectively.

Table 1 – XRF analysis of raw BR, dry basis (normalized)

Composition	Wt%	Composition	Wt%
CaO	9.98	TiO_2	5.67
MgO	0.26	Na_2O	3.51
SiO_2	8.05	K_2O	0.10
Al_2O_3	24.94	P_2O_5	0.13
Fe_2O_3	46.20	SO_3	1.07
MnO	0.09	**Total**	**100**

*Excluding Loss of Ignition (LOI)

Table 2 – XRF analysis of raw $CaCO_3$ powder, dry basis (normalized)

Composition	Wt%	Composition	Wt%
CaO	98.632	TiO_2	0.005
MgO	0.547	Na_2O	0.037
SiO_2	0.208	K_2O	0.035
Al_2O_3	0.175	P_2O_5	0.009
Fe_2O_3	0.084	SO_3	0.263
MnO	0.005	**Total**	**100**

*Excluding Loss of Ignition (LOI)

Table 3 – XRF analysis of sintered BR pellet

Composition	Wt%	Composition	Wt%	Composition	Wt%
CaO	29.01	Cr_2O_3	0.18	P_2O_5	0.12
MgO	0.37	V_2O_5	0.15	SO_3	1.03
SiO_2	7.66	TiO_2	3.87	ZrO_2	0.11
Al_2O_3	23.12	NiO	0.06	SrO	0.03
Fe_2O_3	30.52	Na_2O	3.61	Co_3O_4	0.02
MnO	0.04	K_2O	0.10	**Total**	**100**

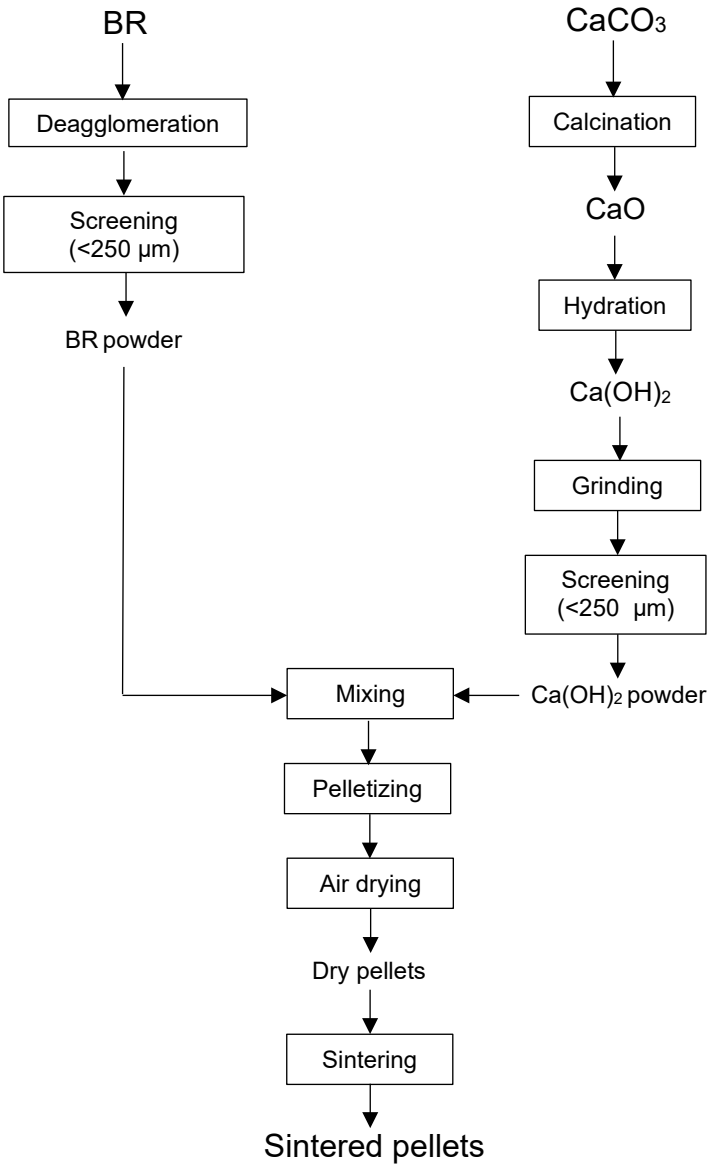

FIG 1 – Flowsheet of the pelletizing and sintering process.

H_2 Reduction

The reduction experiments were conducted using a vertical alumina tube resistance furnace with an outer metallic alloy heating element. Around 20 grams of sintered pellet was used in every experiment. Shown in FIG 2 is both the furnace and a schematic of its inside. The furnace consists of a cylinder-shaped alumina tube, surrounded by an element that is twined around the furnace. A thermocouple is inserted from the top of the furnace to measure the temperature of the sample holder. The sample holder is made from alumina with gas distributor attached at the bottom to ensure uniform gas distribution to the sample bed. The furnace features a reduction gas inlet positioned at its lower section which goes directly to the sample holder, while the gas, having interacted with the sample, is subsequently leaves through the top gas outlet of the furnace. Another gas inlet at lower section of the furnace which does not go to the sample holder is used to flush the furnace with Argon gas at all times of the experiment to prevent water vapor accumulation in the furnace chamber. The heating and cooling were programmed, while the temperature changes were collected by data logging.

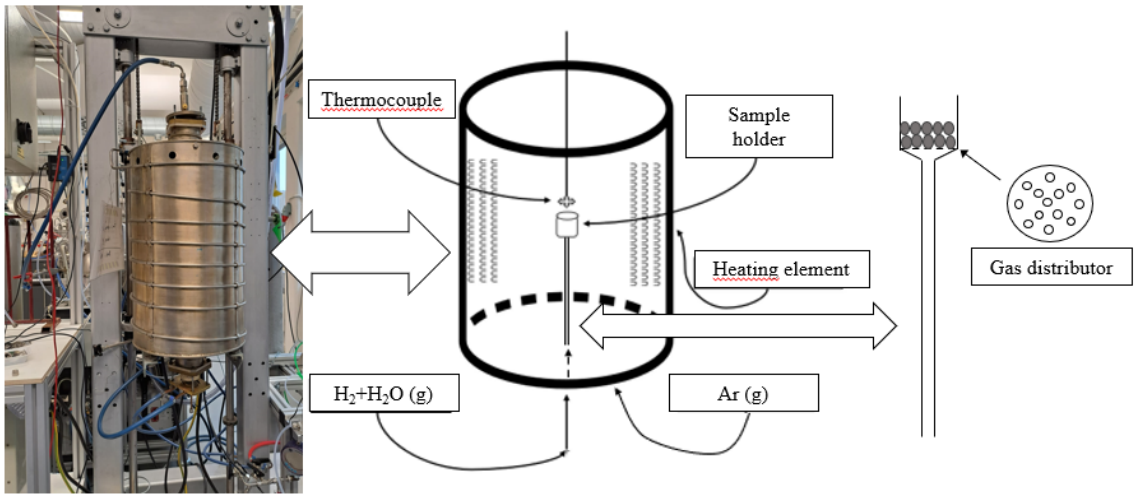

FIG 2 – Picture and schematic diagram of reduction furnace

H_2-H_2O gas mixture composition was controlled by flowing H_2 gas through a humidifier with set humidity value. The humidifier is P-10 model made by Cellkraft™ AB with membrane technology. Experiments were done in 3 different H_2-H_2O gas compositions at 600 °C as shown in Table 4. Heating rate of the furnace was 10 °C/minute and held for 2 hours at set reduction temperature. Total flow of H_2-H_2O gas mix was kept at 1 L/min at all experiments and the furnace was flushed with 1L/min of argon at all times, including the cooling and heating period. Schematic heating diagram of the experiment is shown in FIG 3.

.

Table 4 – Experiment conditions for H_2 reduction

No.	Gas composition (vol %)	Reduction temperature (°C)
1	95% H_2 – 5% H_2O	600
2	85% H_2 – 15% H_2O	600
3	75% H_2 – 25% H_2O	600

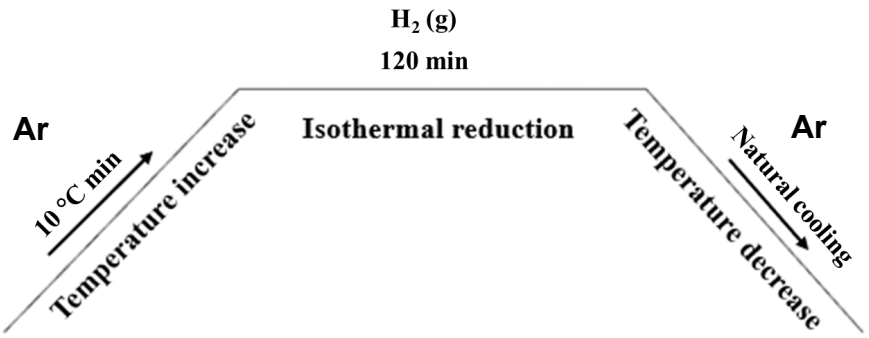

FIG 3 – Heating diagram of H_2 reduction experiment

Thermal Analysis

To simulate a smelting process, samples from sintered and reduced BR were subjected to heat treatment up to 1400 °C under inert atmosphere. A single pellet from each hydrogen reduction experiment and the sintered pellet were grinded and sieved to < 1mm in preparation for DTA and TGA analysis. Two hundred milligrams of sample were used for every analysis. Both DTA and TGA analysis were carried out at the same time using LINSEIS™ TG-DTA equipment by putting the sample inside an alumina crucible. It is expected that the surface of alumina crucible which is in contact with the sample might react with the sample, promoting reactions with alumina as reactant or hindering reactions with alumina as product. However, considering the alumina content in the sample, although quantitative analysis on the result would be inaccurate due to reaction between the sample and the alumina crucible, it should not incur major interference in qualitative analysis.

The analysis was carried out under argon flow of 27.8 cc/min for the whole time with heating rate of 20 °C/min up to 1000 °C and 10 °C/min from 1000 °C to 1400 °C. The sample was cooled naturally inside the furnace with argon flow of 27.8 cc/min.

RESULTS AND DISCUSSION

XRD Analysis

XRD analysis for sintered BR pellets and those reduced at 600 °C is shown in FIG 4. Major phases in the sintered pellets were Brownmillerite ($Al_{0.441}Ca_2Fe_{1.559}O_5$), Gehlenite ($Al_2Ca_2O_7Si$), Lawsonite ($Al_2CaO_{10}Si_2$), Wollastonite ($CaO_3Si$), Melilite($Ca_{5.95}Na_{2.05}O_{15}Si_4$), Perovskite ($CaTiO_3$) and Hematite ($Fe_2O_3$). Meanwhile major phases in the reduced pellets were Srebrodolskite ($Ca_2[Fe,Al]_2O_5$), Gehlenite ($Al_2Ca_2O_7Si$), Perovskite ($CaTiO_3$), Magnetite (Fe_3O_4), Wüstite (FeO) and metallic iron. Brownmillerite and Srebrodolskite peaks were in similar positions due to their similar chemical composition and both belongs to the Brownmillerite subgroup, but with different crystallography. Based on XRD analysis all the Brownmillerite phase in sintered pellets were transformed into Srebrodolskite during H_2 reduction process. It was also observed that most of the calcium silicate-containing phases in the sintered pellets were absorbed into Gehlenite during H_2 reduction, leaving only Gehlenite as the only calcium silicate-containing phase in reduced pellets.

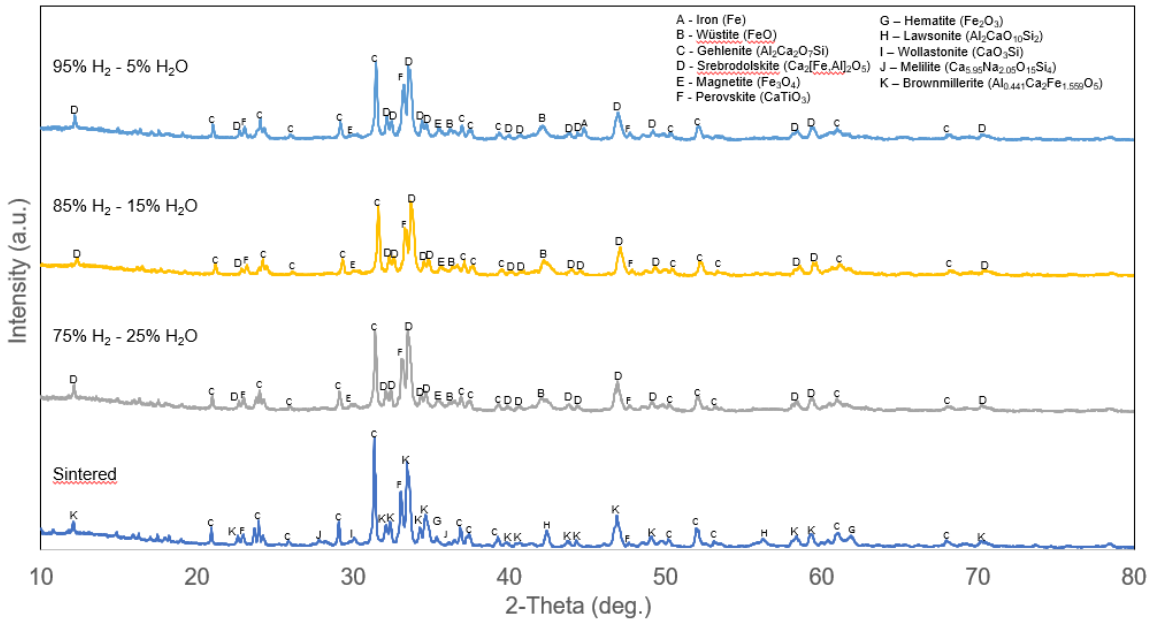

FIG 4 – XRD analysis of sintered BR pellets and pellets reduced at 600°C

By analysing chemical composition of the phases between sintered pellets and reduced pellets it can be concluded that only iron oxides were reduced during H_2 smelting reduction at 600 °C. Magnetite and Wüstite peaks were observed in all the reduced pellets suggesting slow kinetics of the reduction reaction. Meanwhile metallic iron peaks were observed only in pellets reduced with 95% H_2 – 5% H_2O gas composition, suggesting that the equilibrium for reduction of metallic iron at 600 °C exists between 85% to 95% H_2 and 5% to 15% H_2O gas composition.

DTA Analysis

DTA analysis for sintered and reduced BR pellets is shown on FIG 5. There are 12 temperature points of interests which are signified by occurrence of troughs in DTA curves.

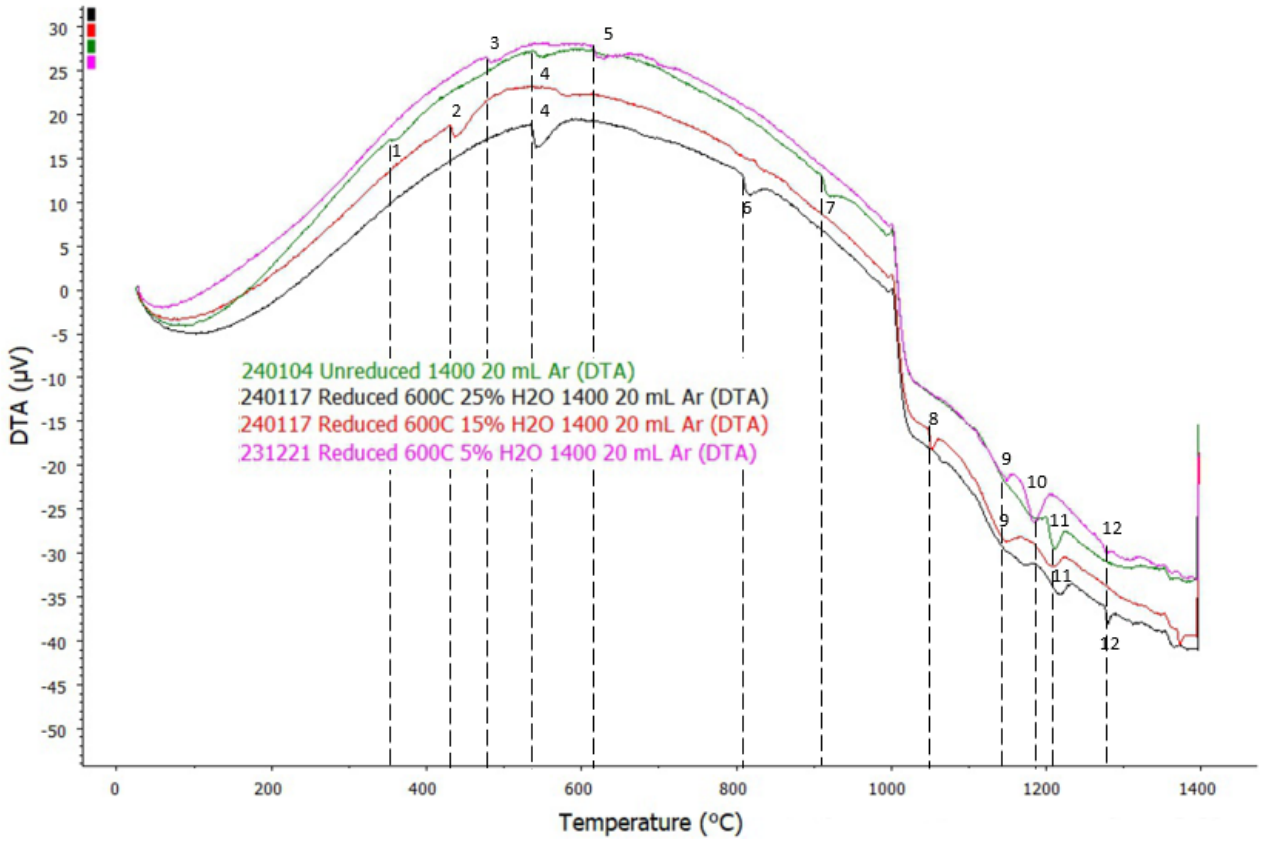

FIG 5 – DTA analysis of sintered BR pellets and pellets reduced at 600 °C

Phase equilibrium module of Factsage™ 8.1 was used to analyse and simulate melting process of sintered and reduced pellets. The simulation for sintered pellets was done based on chemical composition of XRF analysis for sintered pellets as shown in Table 3 in a basis of 100 grams total mass. Whereas for simulation of reduced pellets 10 mol% and 5 mol% of initial Hematite composition in sintered pellets were converted into Wüstite and Magnetite, respectively. Amount of Wüstite and Magnetite for simulation of reduced pellets was estimated based on XRD result of BR pellets reduced at 600 °C with 95% H_2 – 5% H_2O gas composition. Components input for simulation of reduced pellets is shown in Table 5.

Table 5 – Components input for simulation of reduced BR pellets using Factsage™ 8.1

Component	**Mass (gr)**	**Component**	**Mass (gr)**	**Component**	**Mass (gr)**
CaO	29.01	MnO	0.04	P_2O_5	0.12
MgO	0.37	Cr_2O_3	0.18	SO_3	1.03
SiO_2	7.66	V_2O_5	0.15	ZrO_2	0.11
Al_2O_3	23.12	TiO_2	3.87	SrO	0.03
Fe_2O_3	25.94	NiO	0.06	Co_3O_4	0.02
Fe_3O_4	1.48	Na_2O	3.61	**Total**	**99.65**
FeO	2.75	K_2O	0.10		

The simulation was done from 300 °C to 1400 °C to investigate the temperature points of interests in the DTA curves. Resulting Factsage™ 8.1 phase equilibrium simulation for sintered pellets is shown on FIG 6 and result of simulation for reduced pellets is shown on FIG 7.

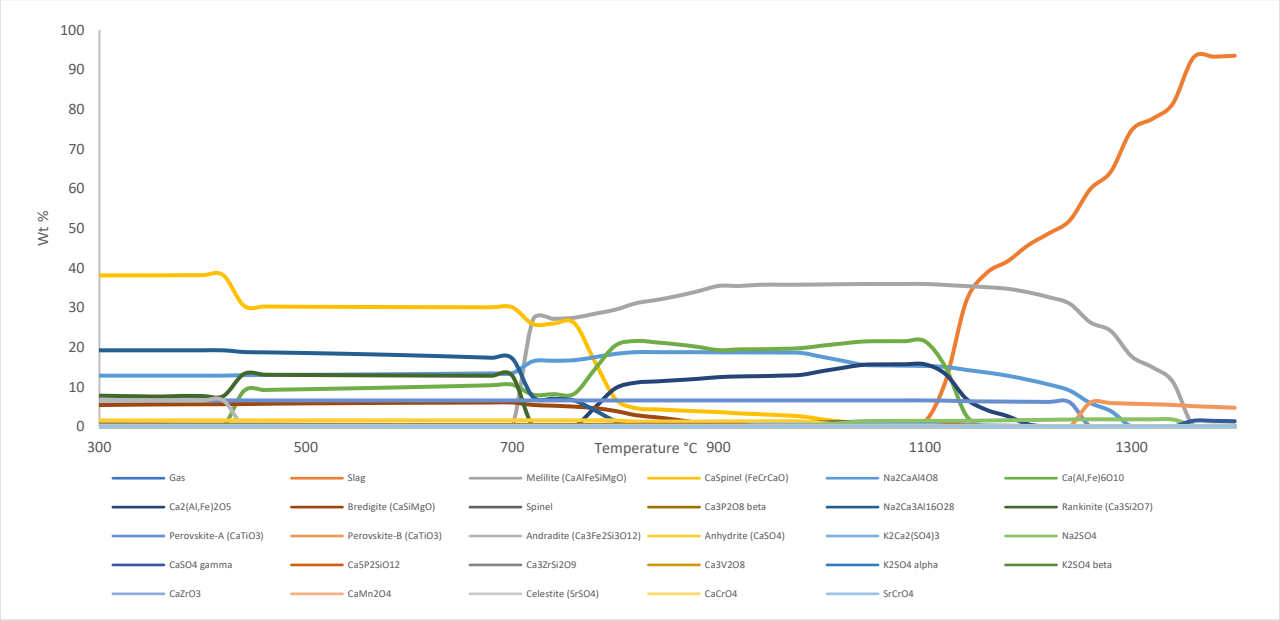

FIG 6 – Phase equilibrium simulation of sintered BR pellets from 300 °C to 1400 °C

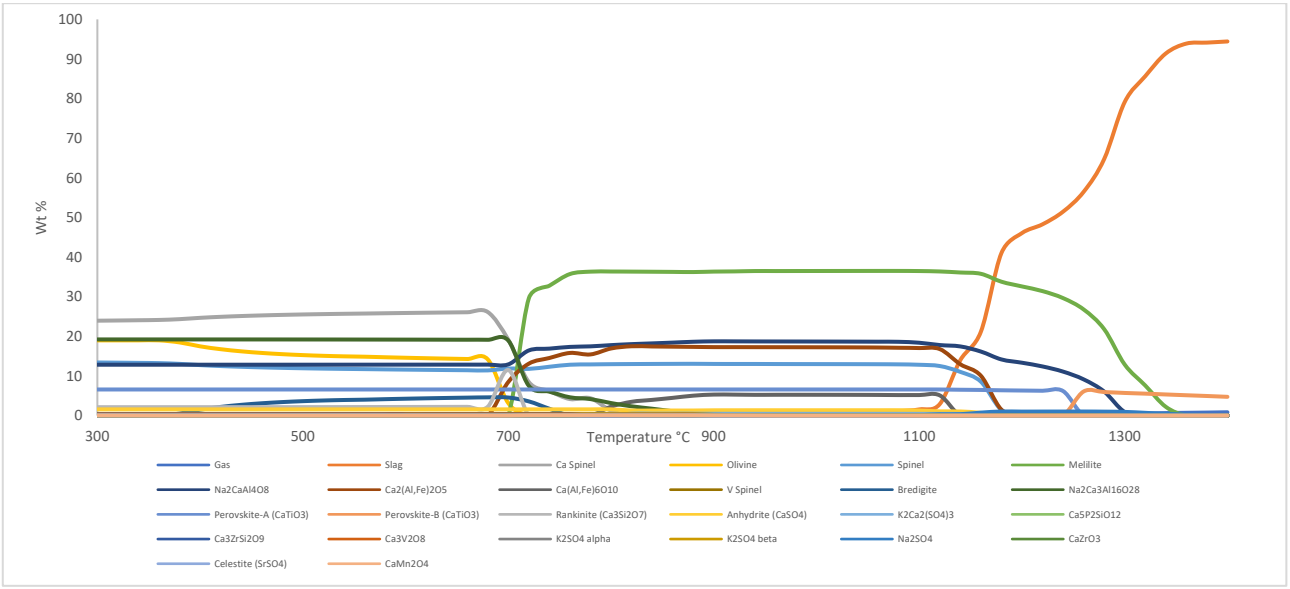

FIG 7 – Phase equilibrium simulation of reduced BR pellets from 300 °C to 1400 °C

The first temperature point of interest occurred at T ≈ 350 °C was signified by occurrence of a small trough in DTA curve of sintered (unreduced) pellet. Based on Factsage™ 8.1 simulation, $Ca_5P_2SiO_{12}$ breaks down into tricalcium phosphate-β (CaP_2O_8) on the first temperature point of interest which is at T ≈ 350 °C. It is proposed that excess calcia and silicon from the reaction immediately dissolved into either Bredigite ($Ca_7Si_4MgO_{16}$) or Rankinite ($Ca_3Si_2O_7$) in the system. The reaction that occurred on this temperature is shown in equation (5).

$$Ca_5P_2SiO_{12} \rightarrow CaP_2O_8 + 4 \cdot CaO + Si \quad (5)$$

Tricalcium phosphate-β is an unstable phase and based on the simulation its reverse reaction occurs at T ≈ 460 °C, which is evidenced by occurrence of crest starting from T ≈ 470 °C on the DTA curve of sintered sample.

The second temperature point of interest occurred at T ≈ 425 °C where a trough occurred on DTA curve of the sample reduced with 85% H_2 – 15% H_2O gas composition. Formation of Bredigite from part of Olivine phase in the sample is supposed to occur around this temperature based on the simulation of sintered pellets. It is possible that olivine reacted with free CaO in the system to form Bredigite with excess magnesium oxide or iron oxide as shown in equation (6).

$$7 \cdot CaO + 4 \cdot (Mg,Fe)_2SiO_4 \rightarrow Ca_7Si_4MgO_{16} + 3 \cdot (Mg,Fe)O \quad (6)$$

The third temperature point of interest at T ≈ 475 °C is signified by occurrence of trough on DTA curve of sample reduced with 95% H_2 – 5% H_2O gas composition. Based on the simulation of reduced pellets a brief formation of Vanadium rich spinel occurred at T ≈ 480 °C, however, it immediately breaks at T ≈ 500 °C which explains the occurrence of trough at this temperature.

The fourth temperature point of interest at T ≈ 540 °C is signified by occurrence of trough on DTA curve of the sintered sample and sample reduced with 75% H_2 – 25% H_2O gas composition. There was another nearby trough occurrence as well on the samples reduced with 85% H_2 – 15% H_2O and 95% H_2 –5% H_2O gas composition, which suggests the same reaction is happening on all samples. Based on the simulation results of both sintered and reduced samples, transformation of potassium sulphate- α (K_2SO_4-α) into potassium sulphate-β (K_2SO_4-β) occurred around this temperature. The reaction is shown in equation (7)

$$K_2SO_4\text{-}\alpha \rightarrow K_2SO_4\text{-}\beta \quad (7)$$

The fifth temperature point of interest is at T ≈ 620 °C, which is signified by occurrence of trough on DTA curve of sample reduced with 95% H_2 – 5% H_2O gas composition. Considering its close proximity with the previous temperature point of interest and the sample is the only one with significant difference in chemical composition compared to other reduced samples, where it is the only one containing metallic Fe. There is a probability that the same reaction occurred where potassium sulphate- α (K_2SO_4-α) transformed into potassium sulphate-β (K_2SO_4-β) since there is no other change occurred in the simulation around 620 °C.

The sixth temperature point of interest at T ≈ 810 °C is signified by the occurrence of trough on samples reduced with 75% H_2 – 25% H_2O and 85% H_2 – 15% H_2O gas composition. From the simulation of sintered samples it was observed that significant formation of calcium alumino ferrite ($Ca[Al,Fe]_6O_{10}$) and Rankinite occurred around this temperature. It is believed that part of Ca-rich spinel in the sample reacted with Andradite ($Ca_3Fe_2Si_3O_{12}$) and CaO in the system to form calcium alumino ferrite and Rankinite as shown in equation (8).

$$3 \cdot CaO + CaFe_2O_4 + 2 \cdot Ca_3Fe_2Si_3O_{12} \rightarrow Ca(Al,Fe)_6O_{10} + 3 \cdot Ca_3Si_2O_7 \quad (8)$$

The seventh temperature point of interest occurred at T ≈ 920 °C, which signified by the occurrence of trough on DTA curve of sintered sample. Based on simulation of sintered sample, Celestite ($SrSO_4$) and $Na_2CaAl_4O_8$ starts to melt around this temperature to form slag phase which may explain the sudden increase in endothermic nature of the system. It is worth noting that Sr content in the sample is quite low hence only a few Sr-containing intermediate phases occurred in the simulation at a very low amount.

The eighth temperature point of interest is at T ≈ 1050 °C, which is signified by occurrence of trough on DTA curve of sample reduced with 85% H_2 – 15% H_2O gas composition. Based on the simulation of reduced pellets, formation of sodium sulfate (Na_2SO_4) are supposed to occur around this temperature. It is proposed that $Na_2CaAl_4O_8$ in the system breaks down to form slag and reacts with free SO_3 in the system to form sodium sulfate as shown in equation (9).

$$SO_3 + Na_2CaAl_4O_8 \rightarrow Na_2SO_4 + 2 \cdot Al_2O_3 + CaO \quad (9)$$

The ninth temperature point of interest at T ≈ 1150 °C is signified by the occurrence of trough on DTA curve of sample reduced with 85% H_2 – 15% H_2O and 95% H_2 – 5% H_2O gas composition which are followed by the occurrence of crest soon after, suggesting exothermic reaction occurred on the system. Based on the simulation of reduced sample a significant amount of calcium alumino ferrite and brownmillerite ($Ca_2[Al,Fe]_2O_5$) broke down to form slag around this temperature, which may explain the exothermic nature of the system.

The tenth and eleventh temperature point of interest is occurring at T ≈ 1180 °C and T ≈ 1220 °C, which is evidenced by occurrence of trough on DTA curve of all the samples. The close proximity between these temperatures suggests that a similar event is happening with small difference in chemical composition of the sample reduced with 95% H_2 –5% H_2O due to presence of metallic iron in it causing the event to occur in a slightly lower temperature compared to others. Based on simulations of both sintered and reduced sample gas phase start to occur around these

temperatures. The release of gas phase from solid components is generally exothermic which may explain formation of trough in the DTA system.

The twelfth temperature point of interest is at T ≈ 1270 °C, which signified by the occurrence of trough on DTA curve of sample reduced with 75% H_2 – 25% H_2O and 95% H_2 – 5% H_2O gas composition. Based on simulation of sintered samples transformation of Perovskite-A into Perovskite-B occurred around this temperature as shown in equation (10).

$$CaTiO_3\text{-}A \rightarrow CaTiO_3\text{-}B \quad (10)$$

Perovskite-A is a very stable phase which relatively remain unchanged from the beginning up to its transformation Perovskite-B. Meanwhile Perovskite-B is less stable than Perovskite-A and as soon as it formed it starts to slowly break down into slag phase.

Based on the simulation, most of the events occurred at each temperature point of interest should apply to all of the samples, however, due to the heterogenous nature of the sample and small amount of sample used in the analysis (~200 mg) obtaining uniform distribution of element in the sample is almost impossible, which explains why some events occurred in one sample but not on the other albeit similar phase composition based on XRD analysis.

TGA Analysis

TGA analysis for sintered and reduced BR pellets is shown on FIG 8.

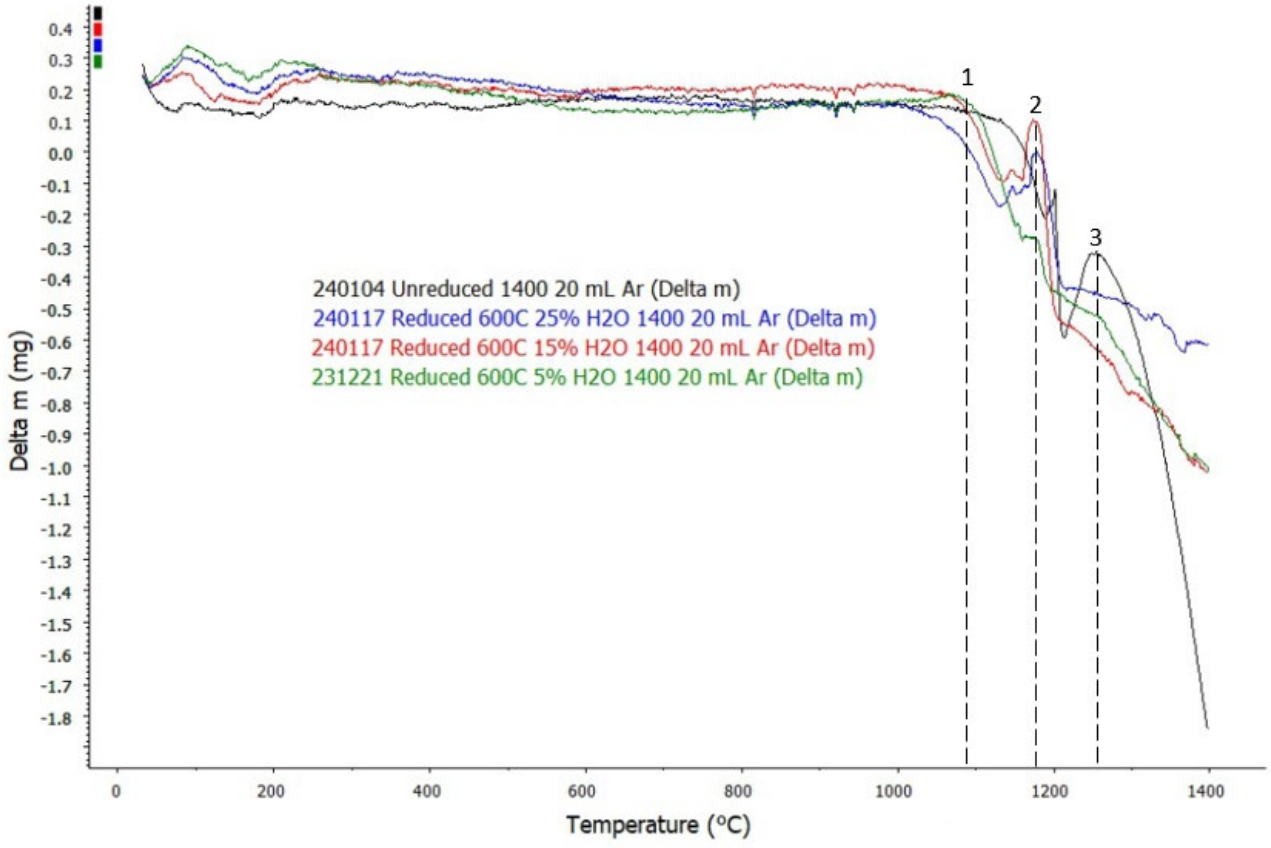

FIG 8 – TGA analysis of sintered BR pellets and pellets reduced at 600 °C.

The curves in FIG 8 showed that there are 3 temperature points of interests where all of them are signified by significant increase in mass loss rate of the samples. All samples, both sintered and reduced, showed the same trend where the first significant increase in mass loss rate occurred at T ≈ 1080 °C, followed by the second significant increase in mass loss rate at T ≈ 1180 °C and the third significant increase in mass loss rate at T ≈ 1280 °C. The same simulation results from Factsage™ 8.1 for sintered and reduced pellets was used to analyse the events happening on same temperature points of interest.

Based on simulation results, liquid slag formation starts to occur at T ≈ 900 °C for both sintered and reduced sample, however, the initial amount is really small since only Celestite and small amount of $Ca_5P_2SiO_{12}$ formed the slag at 900 °C. At this point the slag consists of mostly CaO, CaS, SrO and SrS which originated from Celestite and $Ca_5P_2SiO_{12}$. It is not until T ≈ 1100 °C where the slag starts to pick up iron oxides in the system and increase its amount significantly with increasing temperature. It is proposed that most gases, which are trapped physically in the system are released during this process where larger number of solid phases are getting molten, forming the molten slag phase with lower viscosity and less hold-up potential, subsequently causing the first significant increase in mass loss rate of all systems at the first temperature point of interest which is at T ≈ 1080 °C.

The second temperature point of interest is at T ≈ 1180 °C which correlates to the DTA curve where a trough which followed by crest occurred at similar temperature, as mentioned previously gas phase start to from around this temperature. To properly analyse composition of gas phase with increasing temperature from 1180 °C to 1400 °C another simulation was conducted using Factsage™ 8.1 with addition of 10 litres of argon gas. Similar to simulation of phase equilibrium, components input for sintered pellets was done based on chemical composition of XRF analysis for sintered pellets as shown in Table 3 in a basis of 100 grams total mass and simulation of reduced pellets was done using components input shown in Table 5. Resulting simulation for equilibrium of gas phase composition for sintered pellets is shown on FIG 9 and result of simulation for equilibrium of gas phase composition for reduced pellets is shown on FIG 10.

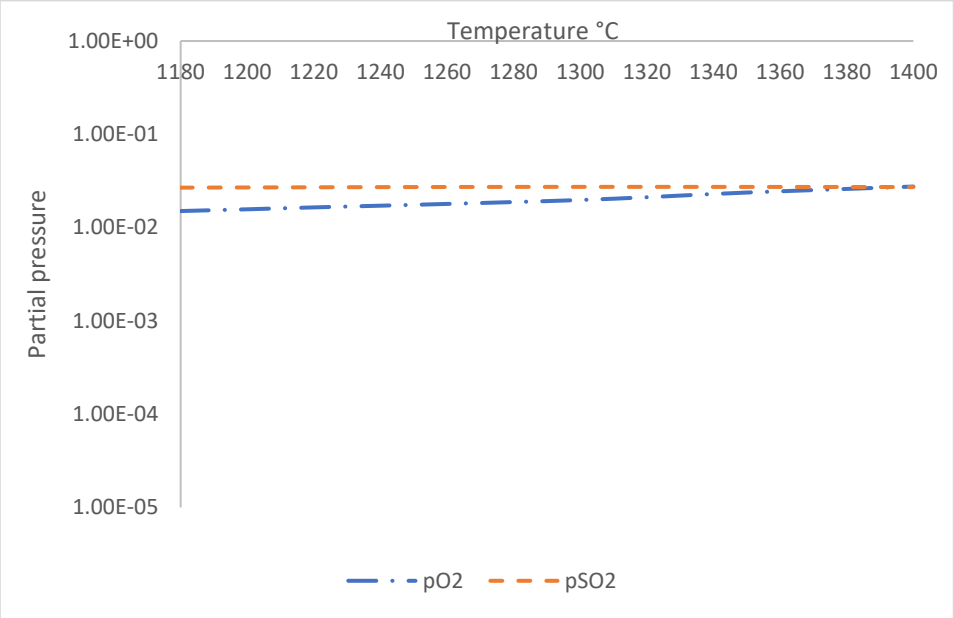

FIG 9 – Equilibrium simulation for gas phase composition of sintered BR pellets from 1180 °C to 1400 °C

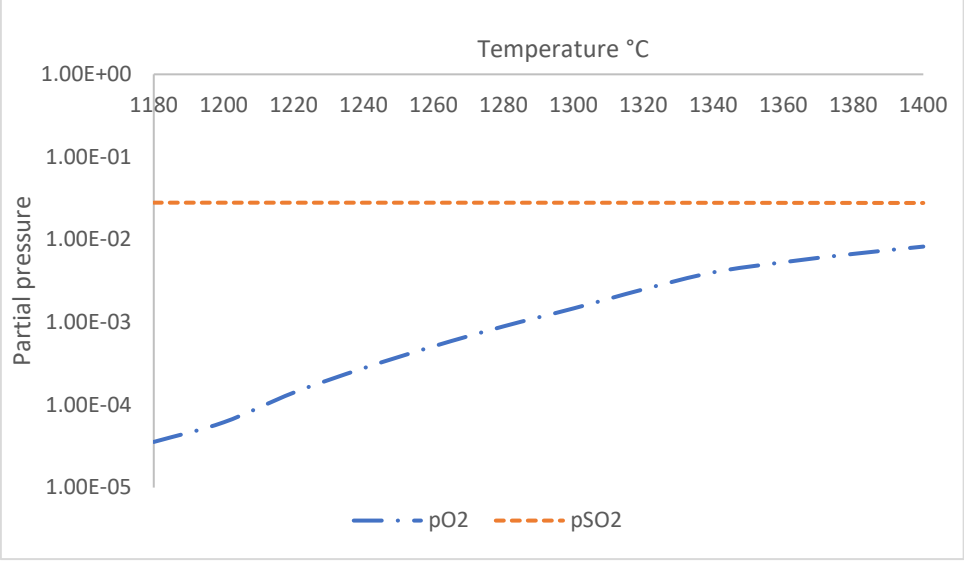

FIG 10 – Equilibrium simulation for gas phase composition of reduced BR pellets from 1180 °C to 1400 °C

Based on simulation gas phase that are discharged by both sintered and reduced samples mainly consists of O_2 and SO_2 gas since partial pressure of other gases such as SO, SO_3, Na_2SO_4 and K_2SO_4 are at least lower by two orders compared to either O_2 or SO_2. Simulation for gas phase composition of sintered sample suggests that both O_2 and SO_2 gas are released at T = 1180 °C meanwhile for simulation of gas phase composition of reduced sample the discharged gas consists of mostly SO_2 at T = 1180 °C since partial pressure of O_2 at this temperature is lower by 3 orders. The difference in gas phase composition is due to reduced samples has significantly less chemically bonded O_2 since more O_2 has been removed during H_2 reduction leaving more chemically bonded SO_2 to be released into the atmosphere in comparison with O2.

Based on the phase equilibrium simulation, the amount of gas phase in sintered samples is supposed to increase significantly with increasing temperature starting from T ≈ 1280 °C and for reduced samples its amount of gas phase start to increase from T ≈ 1260 °C. In correlation, simulation result for gas phase composition of sintered sample showed that partial pressure of O_2 starts to increase more significantly with increasing temperature at T = 1300 °C, suggesting that higher reaction kinetics starts to force higher amount of O_2 gas to be released from the sample despite of oxidative atmosphere due to existing SO_2 gas in the atmosphere, which eventually amplifies gas phase formation with increasing temperature. Simulation result for reduced sample also showed that partial pressure of O_2 is lower by less than one order compared to partial pressure of SO_2 at $T \geq 1320$ °C, increasing the likeliness for remaining O_2 in the sample to be discharged into the atmosphere. It is suggested that increased kinetics of gas phase formation and the release of remaining O_2 from the sample are followed by an increase in mass loss rate of the system which explains the third temperature point of interest at T ≈ 1280 °C.

CONCLUSIONS

1. Transformation of Brownmillerite into Srebrodolskite and dissolution of calcium silicate-containing phases into Gehlenite occurred during H_2 reduction of BR pellets.
2. $Ca_5P_2SiO_{12}$ breaks down into tricalcium phosphate-β (CaP_2O_8), CaO and Silicone at T ≈ 350 °C, however, since tricalcium phosphate-β is an unstable phase, it reverts into $Ca_5P_2SiO_{12}$ at T ≈ 460 °C which are evidenced by corresponding trough and crest on DTA curve of sintered sample.
3. Formation of Bredigite occurred at T ≈ 425 °C where olivine reacted with CaO to form Bredigite. Significant amount of calcium alumino ferrite and Rankinite were formed at T ≈ 810 °C which originates from Ca-rich spinel phase in the system. $Na_2CaAl_4O_8$ in the pellet yields molten slag and reacts with free SO_3 in the system to form sodium sulphate at T ≈ 1050 °C.
4. Transformation of potassium sulphate- α (K_2SO_4-α) into potassium sulphate-β (K_2SO_4-β) occurred at T ≈ 540 °C and transformation of Perovskite-A into Perovskite-B occurred at T ≈ 1270 °C.
5. Initial formation of slag phase for both sintered and reduced pellets occurred at T = °900 C with a small liquid slag formation that contains mostly CaO, CaS, SrO and SrS. Amount of slag phase start to increase significantly with increasing temperature at T ≈ 1100 °C where it starts to pick up iron oxides in the system which then followed by other oxides dissolution/melting in the system.
6. Initial discharge of gas phase from both sintered and reduced pellets occurred at T ≈ 1180 °C where sintered samples started to release both O_2 and SO_2 gas in the system and reduced samples released SO_2 gas. Amount of gas phase for both samples start to increase significantly with increasing temperature starting from T ≈ 1280 °C when increased reaction kinetic forces remaining O_2 in the sample to be released into the atmosphere.

ACKNOWLEDGEMENTS

The current research is funded by HARARE project.

REFERENCES

Borra, R C, Blanpain, B, Pontikes, Y, Binnemans, K and Van Gerven, T, 2016. Smelting of Bauxite Residue (Red Mud) in View of Iron and Selective Rare Earths Recovery, *Journal of Sustainable Metallurgy*, 2, 28-37.

Brunori, C, Cremisini, C, Massanisso, P, Pinto, V and Torricelli, L, 2005. Reuse of a Treated Red Mud Bauxite Waste: Studies on Environmental Compatibility, *J. Hazard. Mater.*, vol.117, no. 1, 55-63.

Ekstroem, K E, Voll Bugten, A, van der Eijk, C, Lazou, A, Balomenos, E and Tranell, G, 2021. Recovery of Iron and Aluminum from Bauxite Residue by Carbothermic Reduction and Slag Leaching, *Journal of Sustainable Metallurgy*, 7, 1314-1326

Kar, M K, van der Eijk, C and Safarian, J, 2022. Hydrogen Reduction of High Temperature Sintered and Self-Hardened Pellets of Bauxite Residue produced via the Addition of Limestone and Quicklime, *Proceedings of 40^{ht} International Conference of ICSOBA*, Athens, Greece, *TRAVAUX* 51, 823-833.

Lazou, A, van der Eijk, C, Tang, K, Balomenos, E, Kolbeinsen, L and Safarian, J, 2021. The Utilization of Bauxite Residue with a Calcite-Rich Bauxite Ore in the Pedersen Process for Iron and Alumina Extraction, *Metallurgical and Material Transactions B*, 52B, 1265.

Liu, X, Han, Y, He, F, Gao, P and Yuan, S, 2021. Characteristic, Hazard and Iron Recovery Technology of Red Mud – a Critical Review, *Journal of Hazardous Materials*, 420, 126542.

Pandey, A K and Prakash, R, 2020. Opportunities for Sustainability Improvement in Aluminum Industry, *Engineering Reports*, e12160.

Samouhos, M, Taxiarchou, M, Pilatos, G, Tsakiridis, P E, Devlin E and Pissas M, 2017. Controlled Reduction of Red Mud by H_2 followed by Magnetic Separation, *Minerals Engineering*, 105, 36-43.

Skibelid, O B, Velle, S O, Vollan, F, van der Eijk, C, Hosseinpur-Kermani, A and Safarian, J, 2022. Isothermal Hydrogen Reduction of a Lime-Added Bauxite Residue Agglomerate at Elevated Temperatures for Iron and Alumina Recovery, *Materials*, 15, 6012.

Smallman, R E and Bishop, R J, 1999. “Chapter 10 – Ceramics and Glasses”, *Modern Physical Metallurgy and Materials Engineering*, 6th Edition, Butterworth-Heinemann, 1999, 320-350.